The Potential of Arsenic-based Zintl Phases as Thermoelectric Materials: Structure & Thermoelectric Properties

Md. Minhajul Islam[1] and Susan M. Kauzlarich[1*]

1: *Department of Chemistry, One Shields Ave, University of California, Davis, CA 95616 USA*

*Corresponding author: smkauzlarich@ucdavis.edu

For the special issue in honor of Eduard Zintl

Abstract

Zintl phase thermoelectric materials have generated tremendous interest due to possessing structural features conducive to high thermoelectric performances. On the other hand, both arsenic and arsenic-based compounds have become attractive in electronics due to having interesting properties like narrow bandgap, tunable carrier concentration, and non-centrosymmetric structures. The structure of arsenic compounds plays a telling role in determining their efficiency as thermoelectric materials. They also show the scope to be doped as both p- and n-type conduction providing exciting new materials with applications as a full module. These attributes make them appealing as thermoelectric materials for further research. This short review is an overview of the different structures of arsenic-based Zintl ternary materials that have potential to be excellent thermoelectric materials.

1. Introduction

A thermoelectric material can convert heat directly into electricity due to temperature gradient through the diffusion of charge carriers from the hot side to the cold side. This effect is based on the Seebeck effect. Inversely, electrical power can be converted into temperature gradient due to the Peltier effect.[1] Thermoelectric devices offer advantages like low noise operation, no moving parts and absence of vibration. It also has minimum space requirements compared to combustion engines and compressor-based refrigerators. The first-generation thermoelectric devices, PbTe/tellurium–antimony–germanium–silver (TAGS) materials manufactured by Teledyne, have found plenty of success in outer space missions conducted by NASA (US National Aeronautics and Space Administration) and the Soviet Union. Earlier space missions such as Voyager 1 and Voyager 2 used radioisotope thermoelectric power system. Even modern era space missions Mars

2011 (rover Curiosity, November 2011) and very recent 2020 missions (Perseverance rover, July 2020) have utilized a radioisotope thermoelectric power system. We can confidently say that deep-space probe missions look set to use this technology in the future.[2]

However, the efficiency of thermoelectric devices still has a lot of room for improvement. The efficiency can be improved by increasing the dimensionless figure of merit, *zT*.

$$zT = \frac{S^2 T}{\rho \kappa}$$

The figure of merit equation is shown above, where S is the Seebeck coefficient, T is the absolute temperature in K, ρ is electrical resistivity and κ is thermal conductivity. The Seebeck coefficient is governed by the density of states effective mass, charge carrier concentration, and temperature while thermal conductivity has two parts: the electronic part, and the lattice part. High electrical conductivity enforces a high electronic contribution of thermal conductivity. Although *zT* is a parameter that helps chemists alter the properties of the materials to enhance the thermoelectric properties, the integral *ZT* holds higher significance in terms of device development. As a result, research for new materials compatible with each other as a p-n junction is of paramount importance. Moreover, using lighter materials like arsenic compounds instead of antimony and bismuth compounds of the same type might lead to a reduction in the weight and cost of payload design while maintaining the same performance.[3]

One approach is to maximize *zT* by lowering the carrier concentration-independent phonon thermal conductivity of the materials. Additionally, the phonon glass and electron crystal concept has been used to design thermoelectric materials where the charge carriers can transport effectively similar to a perfect crystal while the phonon propagation is inhibited as in a glass. All the factors point towards the importance of the material's structure in designing highly efficient thermoelectric materials.[1] For instance, arsenic-based Zintl compounds like $Eu_{14}MnAs_{11}$ and $Eu_{14}CdAs_{11}$ have disorder in their arsenic polyanions.[4,5] This should lead to lower lattice thermal conductivity in arsenic compounds compared to antimony or bismuth ones. Moreover, Justl et al. reported wider bandgap in arsenic-containing compounds compared with antimony or bismuth compounds.[6] The greater implications of increased bandgap might be a higher Seebeck coefficient at higher temperatures for arsenic-containing compounds.

Arsenic, like some other pnictogens, has garnered strong interest due to its structural variations and unexplored applications. Though bulk arsenic has been investigated comprehensively, monolayer arsenic has been reported only recently in the literature.[7] Arsenic can be found in three allotropes: metallic gray, yellow, and black arsenic with gray being the most common and stable form.[8] Recent work have shown that bulk arsenic (black) is a direct bandgap semiconductor with a narrow bandgap of 0.3 eV.[9] On the other hand, the monolayer arsenic (black) is an indirect bandgap semiconductor with an energy gap of about 1–1.5 eV.[7] Small amounts of Arsenic substitution into black Phosphorus provide a Power Factor (S^2/ρ) as high as 316 μV/mK for As_xP_{1-x} with $x = 0.5$.[10] However, grey arsenic has high thermal conductivity of 50.2 W/mK according to Lange's handbook of chemistry.[11] This is an intrinsic drawback making its usage as a thermoelectric material unlikely.

An important arsenic-based compound used in electronics is GaAs. GaAs is a direct bandgap semiconductor having a measured bandgap of 1.4 eV.[12] It showed promising thermoelectric properties such as high mobility of carriers and low thermal conductivity.[13] Consequently, GaAs nanowires showed an impressive zT of 1.34 in a study combining density functional theory (DFT) approaches with the nonequilibrium Green's function (NEGF) method.[14] However, thin film GaAs has not yet lived up to these expectations as it is reported to have a maximum zT of 0.03.[13] Re_3GeAs_6 , of the Ir_3Ge_7 structure type, shows promise with n-type behavior and high Seebeck, low resistivity, but the high thermal conductivity gives rise to a relatively low zT of 0.25.[15] Despite the interest and intrigue of arsenic and its compounds in electronics and thermoelectrics, arsenic is associated with a reported history of toxicity and acute poisoning.[16] Arsenic is classified by the International Agency of Research on Cancer (IARC) as a class I carcinogen for both acute and chronic toxicity on the basis of degree of exposure.

Very few arsenic-containing Zintl phase materials have been studied for their thermoelectric properties, but they are likely good candidates for investigation. Arsenic-containing Zintl phases can be prepared with low dimensional structures, which are expected to show large anharmonicity, typically resulting in low thermal conductivity.[17,18] This review focuses on the potential of As-containing Zintl compounds and highlights the structure and properties of ternary arsenic-based thermoelectric materials as good thermoelectric materials.

2. Zintl Phases

Fritz Laves was the first person to coin the term Zintl phase to refer to a class of compounds comprising a class of intermetallics.[19] Zintl phases are traditionally charged balanced salt-like structures made of alkali or alkaline earth metals and elements from groups 13 to 15. But this definition could be too limiting due to the plethora of compounds discovered later rendering the transition between salt-like and metallic vague. An more useful definition for Zintl phase that works remarkably well is where electron transfer is considered to be essentially complete between the alkali or alkaline earth cation and the electronegative anions that form networks, chains, planes, or clusters to satisfy the octet or 8-N rule.[20] The electron donor cations are located within the interstitial sites serving as guest atoms in the (poly)anionic network.[21] It is important to note that the complete transfer of electrons according to the Zintl concept is a model. Several publications examining the electron density or electron localization in Zintl phases indicate that the formal charges used by the Zintl model are not realized.[11,22] However, despite this complexity, the Zintl rule enables successful predictions concerning crystal structures and composition.

Zintl phases can be found in many binary phases of alkali or alkaline earth metals with main group metalloids, but numerous ternary compounds have also been synthesized. Zintl compounds are usually semiconductors, however, compounds with metallic character have also been reported. The semiconducting behavior makes Zintl compounds with $A_xB_yC_z$ where A = alkali or alkaline earth; B = main group metal, C = main group element an attractive group of materials for thermoelectric applications.[23] There are many Zintl compositions; however, this review will focus on alkaline earth or rare earth arsenides with *x-y-z* compositions such as 3-1-3, 5-2-6, 14-1-11, 2-1-2, and 2-2-3. Their structural differences are expected to profoundly affect the compounds' thermoelectric properties.

Table 1: As-containing Zintl Phases with Reported *zT*

Material	Structure type	Space Group	Type	Maximum *zT*	Reference
Ca_3AlAs_3	Ca_3AlAs_3	*Pnma*	Not reported	-	[24]
Ba_3AlAs_3	Ba_3AlSb_3	*Cmce*	p-type	0.88 (computed)	[25]

Ba_3GaAs_3	Ba_3GaSb_3	*Pnma*	Not reported	-	[26]
Sr_3AlAs_3	Ba_3AlSb_3	*Cmce*	p-type	0.85 (computed)	[25]
Eu_3InAs_3	Ca_3AlAs_3	*Pnma*	n-type	-	[27]
Sr_3InAs_3	Ca_3AlAs_3	*Pnma*	n-type	-	[28]
Eu_3AlAs_3	Rb_3TlO_3	$P2_1/c$	Not reported	-	[29]
Eu_3GaAs_3	Ba_3AlSb_3	*Cmce*	Not reported	-	[29]
$Eu_5Sn_2As_6$	$Sr_5Sn_2P_6$	*Pbam*	Not reported	0.15	[30]
$Sr_5Sn_2As_6$	$Sr_5Sn_2P_6$	*Pbam*	p-type	3.0 along z direction of the first Brillouin zone (computed)	[31,32]
$Eu_5In_2As_6$	$Ca_5Ga_2As_6$	*Pbam*	n-type	0.29	[33]
$Ca_5Ga_2As_6$	$Ca_5Ga_2As_6$	*Pbam*	p-type or n -type	0.95 (computed)	[34,35]
$Ba_{14}MnAs_{11}$	$Ca_{14}AlSb_{11}$	$I4_1/acd$	p-type	-	[36]
$Eu_{14}MnAs_{11}$	$Ca_{14}AlSb_{11}$	$I4_1/acd$	p-type	-	[5]
$Ca_{14}MnAs_{11}$	$Ca_{14}AlSb_{11}$	$I4_1/acd$	p-type	-	[36]
$Sr_{14}MnAs_{11}$	$Ca_{14}AlSb_{11}$	$I4_1/acd$	p-type	-	[36]
$Sr_{14}GaAs_{11}$	$Ca_{14}AlSb_{11}$	$I4_1/acd$	p-type	-	[37]
$Sr_{14}Zn_{1.33}As_{11}$	$Ca_{14}AlSb_{11}$	$I4_1/acd$	p-type	-	[38]
$Eu_{14}Zn_{1.14}As_{11}$	$Ca_{14}AlSb_{11}$	$I4_1/acd$	p-type	-	[38]
$Eu_{14}CdAs_{11}$	$Ca_{14}AlSb_{11}$	$I4_1/acd$	p-type	-	[4]
$Ca_{14}FeAs_{11}$	$Ca_{14}AlSb_{11}$	$I4_1/acd$	p-type	-	[39]
$Sr_{14}Cd_{1.06}As_{11}$	$Ca_{14}AlSb_{11}$	$I4_1/acd$	p-type	-	[4]
Ca_2CdAs_2	α is Yb_2CdSb_2 Or β is Ca_2CdAs_2	α is $Cmc2_1$ β is *Cm*	Not reported	-	[40]
Sr_2CdAs_2	Yb_2CdSb_2	$Cmc2_1$	Not reported	-	[40]
Ba_2CdAs_2	Yb_2CdSb_2	$Cmc2_1$	Not reported	-	[40]

Eu_2CdAs_2	Yb_2CdSb_2	*Cmc*2$_1$	Not reported	-	[40]
Ba_2ZnAs_2	K_2SiP_2	*Ibam*	Not reported	-	[41]
Sr_2ZnAs_2	ZrBeSi	*P*6$_3$/*mm c*	Not reported		[42]
$Sr_2Zn_2As_3$	$Ba_2Cd_2Sb_3$	*C*2/*m*	Not reported	-	[43]
$Eu_2Zn_2As_3$	$Ba_2Cd_2Sb_3$	*C*2/*m*	Not reported	-	[43]
$Eu_2Cd_2As_3$	$Ba_2Cd_2As_3$	*C*2/*m*	Not reported	-	[44]
$Ba_2Cd_2As_3$	$Ba_2Cd_2As_3$	*C*2/*m*	p-type	-	[45]

2.1. A_3MAs_3 (3-1-3)

Zintl compounds with the general formula A_3MX_3 where A is the alkaline-earth , and M is a Group 13 element, and X is a pnictogen have been extensively researched.[24,27,46] For X = As, A_3MAs_3 phases exhibit five different crystal structure types making it the most diverse in terms of structural arrangements of atoms in the unit cell.

There are fundamental differences among structures of A_3MAs_3 in the interconnectivity of atoms due to the atomic sizes and electronegativities. This results in noticeable variations in the Ba_3AlAs_3, Ba_3GaAs_3, and Ba_3InAs_3 structures.[26] For instance, moving from Al to In for the M atom in the structure, the changes lead to different space groups for the compound. Consequently, the space group of Ba_3AlAs_3 differs from that of Ba_3GaAs_3 and Ba_3InAs_3. While the former crystallizes in the orthorhombic *Cmce* space group, the latter two belong to the orthorhombic *Pnma* space group.[47] The difference in the number of atoms in the unit cell is also worth mentioning as Ba_3GaAs_3 contains a unit cell with fifty-six atoms having Ga_2As_6 units while Ba_3InAs_3 has only twenty-eight atoms in the unit cell containing tetrahedral unis of $InAs_4$ connected through corner forming infinitely long chains.[26]

Similarly, Eu_3MAs_3 phases (M = Al, Ga, and In) show structural differences depending on the element in the M atom. Again, the differences start from the space group of the crystals. Eu_3AlAs_3 adopts the monoclinic structure belonging to *P*2$_1$/*c* space group, but Eu_3GaAs_3 is structurally similar to Ba_3AlSb_3. It belongs to the orthorhombic *Cmce* space group. Another difference arises

from the packing of the Al_2As_6 and Ga_2As_6 units due to their respective extended symmetries.[29] Recently synthesized Eu_3InAs_3 and Sr_3InAs_3 adopt the *Pnma* space group while containing [$InAs_4$] tetrahedra chains like in Ba_3InAs_3.[27]

The A_3MAs_3 composition has structural features to make the compound charge balanced and valence precise. For instance, The $InAs_4$ tetrahedra form a chain, shown in Figure 1, that can be described as edge-sharing tetrahedra with two shared As atoms and two terminal As atoms, giving rise to the formal charge of 6- for the moiety [$InAs_2As_{2/2}$].[27] The oxidation states of the elements can be represented as $[Eu^{2+}]_3[In^{3+}][As^{3-}]_3$. But it is important to remember that this is a very rudimentary way of representing the electron counting. In fact, electrons are shared in the anion moieties rather than complete transfer of the electrons as in ionic compounds. The semiconducting behavior of Eu_3InAs_3 and Sr_3InAs_3 makes them possible candidates as thermoelectric materials. They exhibit intrinsic characteristics with narrow band gaps.

Eu_3InAs_3 shows a negative Seebeck coefficient from 300 to 700 K temperature range. The presence of a large negative Seebeck coefficient is rare for a Zintl phase.[27] To date, most Zintl phases that have been characterized are p-type semiconductors with defects on the cation sites. A negative Seebeck coefficient implies that electrons are the dominant carriers and n-type behavior. This unusual behavior in Zintl compounds suggest that there are minimal vacancies on the cationic sites combined with excess electrons from the anionic component. In any undoped compound, electron dominated charge transport is due to native defect chemistry. In the case of Yb or Eu cations, defects might arise from the variation in the valence state of Yb or Eu between 2+/3+. These compounds have not been experimentally measured for their thermoelectric properties.

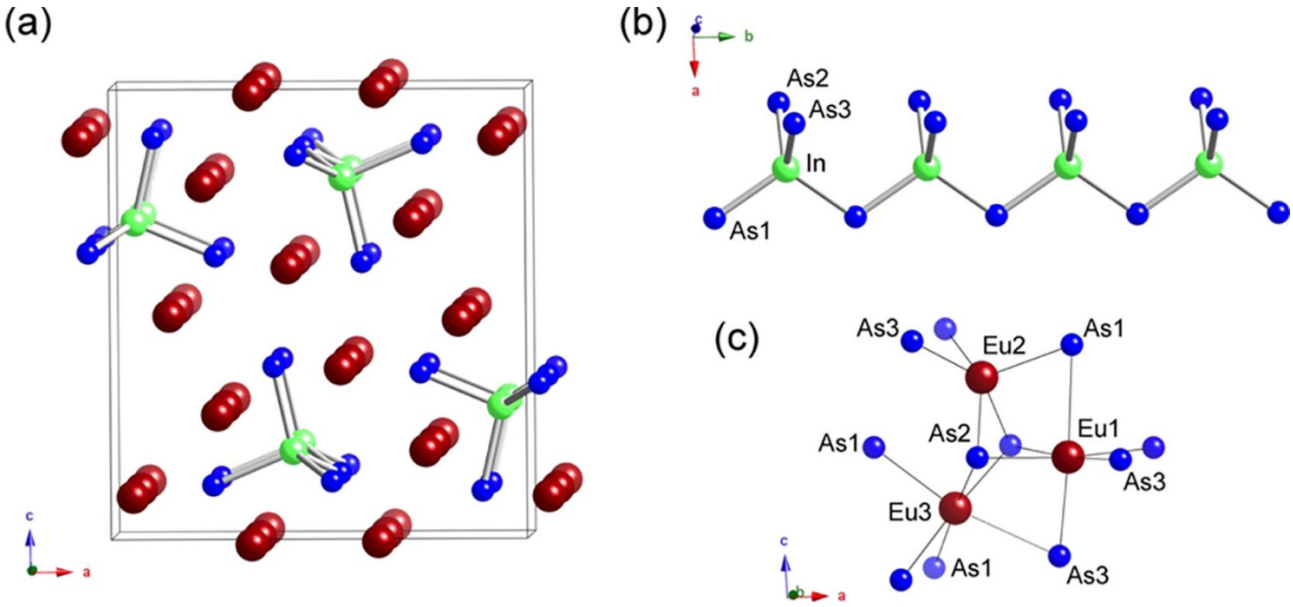

Figure 1. (a) The structure of Eu_3InAs_3 is shown where Eu atoms are represented by red sphere, In represented by green sphere, and As represented by blue sphere. (b) A chain of $[InAs_4]^{6-}$ is formed by corner-sharing $[InAs_4]$ tetrahedra (c) Eu1, Eu2, and Eu3 atoms have different coordination environments. Reprinted from [27] with permission. Copyright 2020 from American Chemical Society.

2.2. $A_5M_2As_6$ (5-2-6)

$Ca_5Sn_2As_6$-type structure ($A_5M_2As_6$) was discovered more than 30 years ago where A could be divalent alkaline-earth or rare-earth element like Ca, Sr, Eu, and Ba and M could be Cd or Zn.[48]

5-2-6 compounds have three structure types reported as $Ca_5Ga_2As_6$, $Ba_5Al_2Bi_6$, and $Sr_5Sn_2P_6$ respectively.[49] The Ca and Ba containing structures have different coordination of the cations in an otherwise identical structure. The cation Ca is an ideal octahedral geometry in $Ca_5Ga_2As_6$. On the other hand, Ba is in a distorted octahedral geometry in $Ba_5Al_2Bi_6$. More recently, some compounds such $A_5Cd_2As_6$ and serendipitously synthesized $A_5Sn_2As_6$ have sparked interest. Among them, both $Sr_5Sn_2As_6$ and $Eu_5Sn_2As_6$ adopt the $Sr_5Sn_2P_6$ structure type.[30]

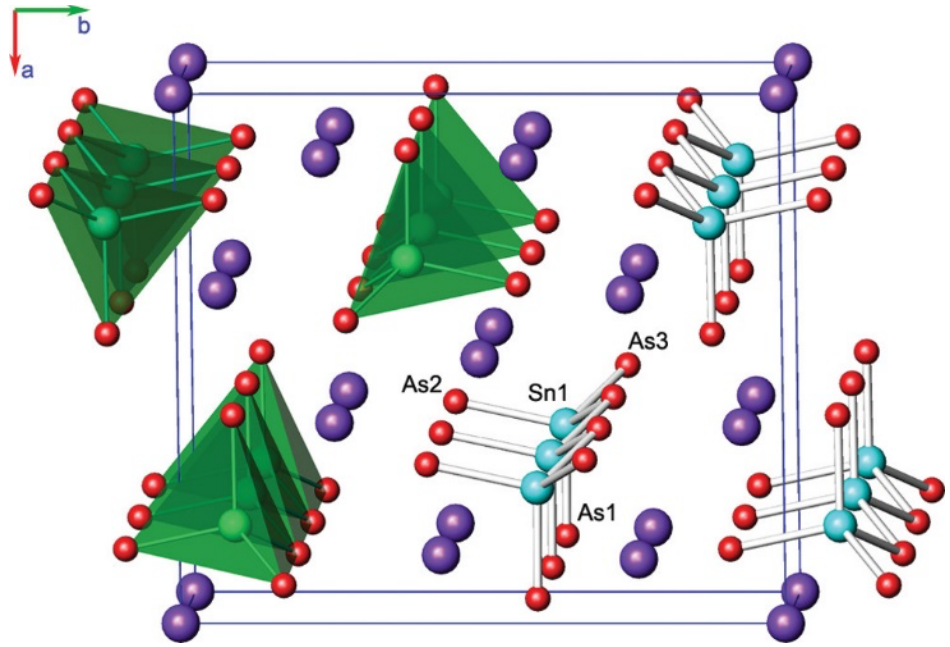

Figure 2. In the $Sr_5Sn_2As_6$ structure, centers of As tetrahedra contain Sn atoms represented by light-blue spheres. Arsenic atoms are represented by red spheres. The vacant space in-between the $[Sn_2As_6]$ chains are filled by the purple spheres of Sr cations. Reprinted from [30] with permission. Copyright 2012 from American Chemical Society.

The Zintl−Klemm concept can be applied to understand the electron counting of $Sr_5Sn_2As_6$.[32] The elements' formal oxidation states (Sr^{2+}, Sn^{4+}, and As^{3-}) make the compound a charged-balanced Zintl phase with $(Sr^{2+})_5(Sn^{4+})_2(As^{3-})_6$. Employing the 8-N rule, with chemical bonding included provides $[Sr^{2+}]_5$[4 bonded $Sn^0]_2$[2 bonded $As^{-1}]_2$[1 bonded $As^{2-}]_4$. The structure is shown in Figure 2, where 1D chains formed by $SnAs_4$ tetrahedra via sharing the corners propagate in the *c*-direction [001]. There are three independent Sr^{2+} cations: Sr1, Sr2, and Sr3. Sr2 is coordinated to seven As^{3-} anions. On the contrary, Sr1 and Sr3 strontium atoms occupy distorted octahedra formed by six arsenic atoms. Thus, the strontium ions fill the cavities among the tetrahedral chains. The bond lengths between strontium and arsenic atoms range from 3.10 to 3.37 Å.

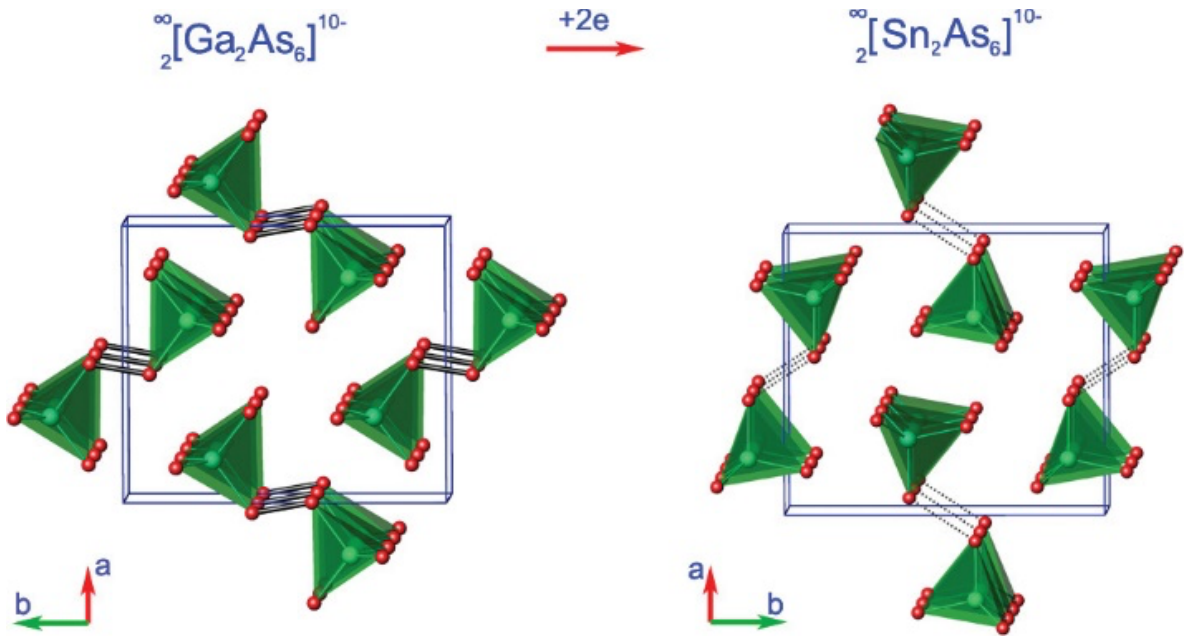

Figure 3. A view of the crystal structures of $Ca_5Ga_2As_6$ and $Sr_5Sn_2As_6$ showing the difference between the $[Ga_2As_6]^{10-}$ and $[Sn_2As_6]^{10-}$ connectivity. Reprinted from [30] with permission. Copyright 2012 from American Chemical Society.

Despite having the 5-2-6 composition, $Ca_5Ga_2As_6$ and $Sr_5Sn_2As_6$ have structural differences. From Figure 3, both structures have one-dimensional chains with corner-sharing MAs_6 tetrahedra where M is Ga or Sn. The notable difference arises from the chain formed by the polyanions where $[Ga_2As_6]^{10-}$ has arsenic-arsenic dimers connecting two $[GaAs_3]$ single chains resulting in a double-chain structure. In contrast, $[Sn_2As_6]^{10-}$ has two separate $[SnAs_3]$ chains with arsenic-arsenic bonds. The distance between As-As bond between two chains in $[Ga_2As_6]^{10-}$ is 2.49 Å whereas it is 3.32 Å in case of $[Sn_2As_6]^{10-}$.[30,50]

Recently synthesized $Eu_5In_2As_6$ adopts the orthorhombic $Ca_5Ga_2As_6$ structure. It belongs to the space group *Pbam*. Based on the Zintl formalism, the compound is charge balanced. The oxidation states of the elements can be represented as $(Eu^{2+})_5(In^{3+})_2(Pn^{3-})_4(Pn^{2-})_2$.[29] Along the *c* axis shown in Figure 4, $[InPn_4]$ tetrahedra form the strands by being linked through the corners. Eu atoms reside in between these polyanions. As-As bonds connect the strand into double strands with a bond distance of 2.51 Å.

Unlike most Zintl compounds that are p-type, the negative Seebeck coefficients and Hall coefficients confirm that $Eu_5In_2As_6$ is an n-type semiconductor.[33] Doping with La or Zn has a

contrasting effect on the material's carrier type as La^{3+} donates electrons compared with Eu^{2+} while Zn^{2+} is electron deficient compared with In^{3+}. As a result, the La doped phase remains n-type but the Zn doped material acts as a p-type semiconductor. The thermoelectric measurements of the pristine phase reveal a low Seebeck coefficient of -32 μV K^{-1} at 300 K. This is attributed to the multicarrier nature of the material. The bipolar nature of the conductivity has a telling effect on the Seebeck coefficient at higher temperatures, suggesting that with optimal doping an efficient n- and p-type thermoelectric material might be realized. Contrary to the impact on the Seebeck coefficient, the thermal conductivity is negligibly affected by the bipolar nature of the conductance. It is in the low range of 1.6 W m^{-1} K^{-1} at 300 K due to bonding anharmonicity and complex structure. As chemical bonding affects atomic vibrations to impact transport properties, the presence of strongly anharmonic bonding could lead to very low lattice thermal conductivity.[51] Though the electrical resistivity of the pristine phase is 7.2 Ω cm, the maximum *zT* of 0.29 is obtained for the Zn-doped material. Similarly, $Eu_5Sn_2As_6$ also exhibits a low *zT* of 0.15 after doping with K.[52]

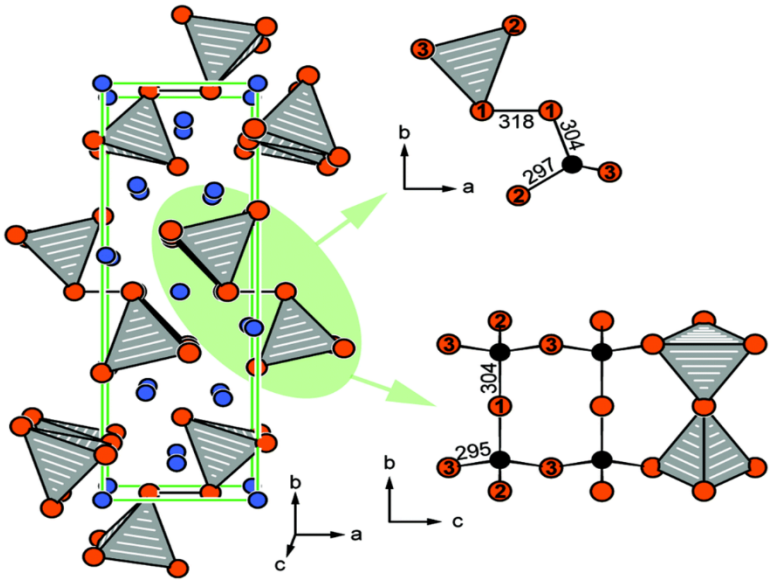

Figure 4. The structure of $Eu_5In_2As_6$ (left) shows the presence of [$InAs_4$] tetrahedra. [$InAs_4$] tetrahedra form double strands depicted along [001] (right top) and [100] (right bottom). The numbers between the arsenic atoms are interatomic distances given in pm. Blue circles represent Eu, black circles represent In and orange circles represent As atoms. Reprinted from [29] with permission. Copyright 2020 from Royal Society of Chemistry.

A theoretical study of the thermoelectric properties of $Sr_5Sn_2As_6$ reveals large Seebeck coefficient is responsible for *zT* of 1.0 at 800 K before doping. Further study with n-type doping results in a calculated *zT* of 3.0 along the *z*-direction of the Brillouin zone at 950 K. This can be attributed to large Seebeck coefficient and high electrical conductivity along the *z*-direction due to the presence of larger degeneracy and lighter bands along *Γ*-*z*.[32] Similarly, a computational study on $Ca_5Ga_2As_6$ reveals a maximum zT of 0.95 for p-type doping along the z-direction of the first Brillouin zone.[35]

2.3. $A_{14}MAs_{11}$ (14-1-11)

Zintl compounds with the tetragonal crystal system $A_{14}MPn_{11}$ (where A is divalent electropositive metals Ca, Sr, Ba, Eu, or Yb; M is Al, Ga, In or transition metal such as Mn, Zn or Cd; and Pn represents pnictogens like P, As, Sb, Bi) have generated a great deal of interest because of their exclusive properties suitable for thermoelectric applications. To date, the thermoelectric properties of the arsenic analogs have not been experimentally measured. $Ca_{14}GaAs_{11}$ was the first example of a 14-1-11 structure containing arsenic where $GaAs_4$ tetrahedron did not form any $GaAs_4$ network.[53]

Many other arsenic-based 14-1-11 structure compounds were reported including $Ba_{14}MnAs_{11}$,[36] $Ca_{14}FeAs_{11}$,[39] $Ca_{14}MnAs_{11}$,[36] $Sr_{14}GaAs_{11}$,[37] $Sr_{14}Zn_{1.33}As_{11}$,[38] and $Sr_{14}Cd_{1.06}As_{11}$.[4] $Ca_{14}FeAs_{11}$,[39] is the first example of M = Fe for compounds for this structure type. The presence of Mg and transition metals as M with divalent charge and nonstoichiometric compositions show the existence of non-electron precise Zintl compounds. These compounds are shown to be p-type semiconductors with carrier concentrations consistent with one electron deficiency.

All of them crystallize in the tetragonal crystal system with space group $I4_1/acd$.[4] The structure of the compounds can be described as containing $[MAs_4]$ tetrahedra, either a linear $[As_3]$ anion, and isolated As atoms. The average arsenic-arsenic bond length is 2.76 Å. The stoichiometry and nonstoichiometric in compounds with 14-1-11 composition can introduce structural differences. For instance, the presence of interstitial M atoms in the structure is reported for $Eu_{14}Zn_{1.14}As_{11}$ and $Sr_{14}Cd_{1.06}As_{11}$ but not for $Eu_{14}CdAs_{11}$.[4,38] This was attributed to clusters formed by the robust cation–cation interactions. This augments the total electron counts and compensates for election deficiency.

More recently, a 14-1-11 compound $Eu_{14}AlAs_{11}$ was prepared using elemental europium, arsenic, and aluminum.[54] $Eu_{14}AlAs_{11}$ crystallized in the tetragonal crystal system having space group $I4_1/acd$. The lattice parameter a is 16.28 Å and c is 21.80 Å in the case of arsenide. The $Eu_{14}AlAs_{11}$ Zintl phase can be described as a transfer of 28 electrons calculated from the ionic components represented by $(Eu^{2+})_{14}(AlAs_4^{9-})(As^{3-})_4(As_3^{7-})$ with $[AlAs_4]^{9-}$ being a tetrahedral anion and $[As_3]^{7-}$ being a linear anion. The tetrahedral anion $[AlAs_4]^{9-}$ can be written as $[Al]^{3+}$ and $[As^{3-}]_4$ whereas linear polyanion $[As]^{7-}$ can also be described as a dimer $[As_2]^{4-}$ dumbbell and isolated $[As]^{3-}$ anions. Therefore, the charged balanced ionic characterization of the structure can be represented by $(Eu^{2+})_{14}[(Al^{3+})(As^{3-})_4](As^{3-})_4(As_3^{7-})$. The 8-N description, including the chemically bonded units can be written as [4 bonded Al^{-}][1 bonded $As^{2-}]_4$[0-bonded $As^{3-}]_4$[1 bonded $As^{2-}]_2$[0-bonded As^{3-}]. It is important to note that the Pn_3^{7-} anions found in 14-1-11 compounds contain are isoelectronic with triiodide anions with 3c-4e bonds, consistent with valence bond theory.

From Figure 5, the unit cell showed the presence of isolated Pn^{3-} and tetrahedral $[AlAs_4]^{9-}$ anions along with As_3^{7-} anions. One more europium arsenides with this composition is $Eu_{14}MnAs_{11}$.[5] None of these arsenide compounds have been experimentally investigated for thermoelectric properties.

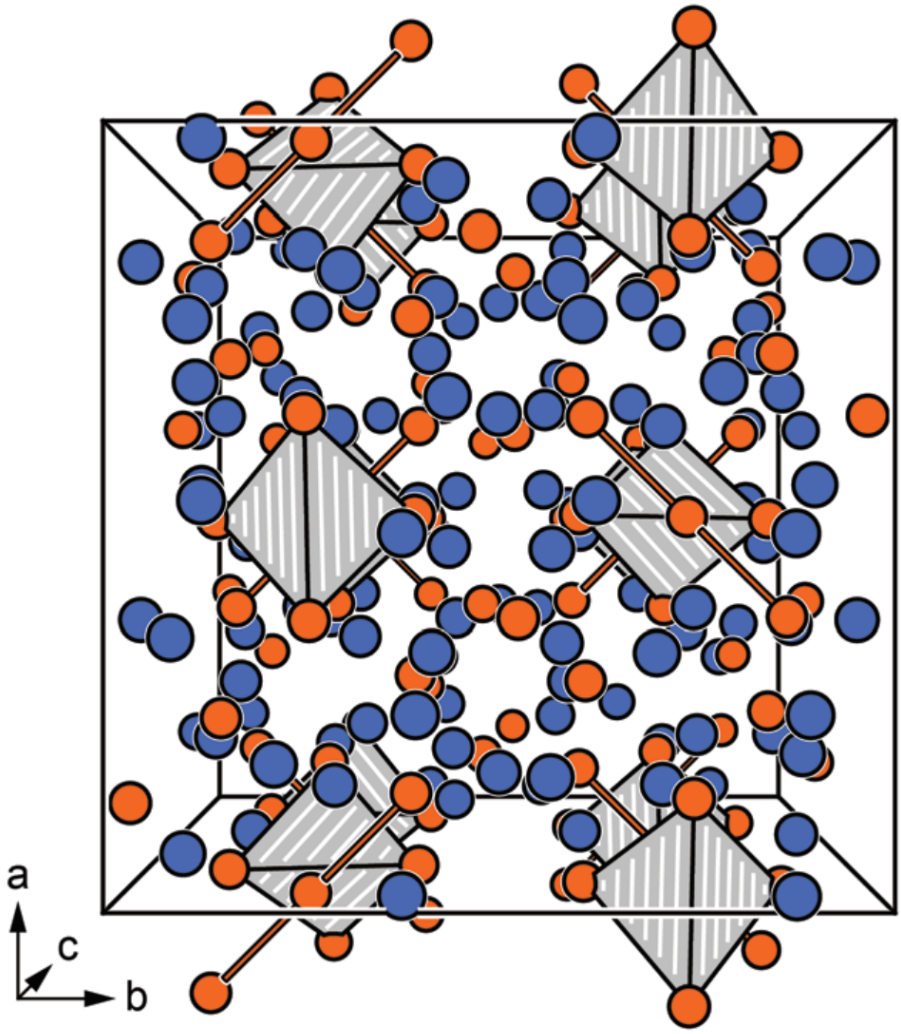

Figure 5. The structure of $Eu_{14}AlAs_{11}$ along [100]. The bonding within the As_3^{7-} tri-pnictide and the tetrahedral coordination environments of the $[AlAs_4]^{9-}$ surrounding the Al atoms are highlighted. Blue circles represent Eu atom, white circles represent Al atoms and orange circles represent As atoms. Reprinted from [54] with permission. Copyright 2014 from Royal Society of Chemistry.

A systematic study of arsenic incorporation into the $Yb_{14}MgSb_{11}$ by gradually replacing Sb atoms using first-principles electronic structure calculations was reported.[55] The positive impact of substitution by As atoms on the Seebeck effect at higher temperatures is revealed. Due to increased effective mass, the Seebeck coefficient of $Yb_{14}MgSb_{11}$ increased as Sb atoms were substituted by As atoms. This theoretical study showed that As containing Zintl compounds of $A_{14}MAs_{11}$

composition might be as good as, if not better than, the class leading antimonide 14-1-11 compounds.

2.4. A_2MAs_2 (2-1-2)

Compounds with a 2-1-2 structure have been synthesized such as Ca_2CdAs_2, Sr_2CdAs_2, Ba_2CdAs_2, and Eu_2CdAs_2.[56] There are two polymorphs of Ca_2CdAs_2: β-Ca_2CdAs_2 with a monoclinic structure, while α-Ca_2CdAs_2 is orthorhombic. Due to the difference in the stability of the polymorphs at higher temperatures, β-Ca_2CdAs_2 forms at higher temperatures while α-Ca_2CdAs_2 is favored at lower temperatures.

α-Ca_2CdAs_2, Eu_2CdAs_2, Sr_2CdAs_2, and Ba_2CdAs_2 adopt the orthorhombic $Cmc2_1$ and β-Ca_2CdAs belongs to the *Cm* space group. For Ca_2CdAs_2, both polymorphs have layers connected through the corners of $CdAs_4$ tetrahedra.[56]

Though both β-Ca_2CdAs_2 and α-Ca_2CdAs_2 have $CdAs_4$ tetrahedra with different features, the β phase has distorted tetrahedra with Cd-As bonds ranging from 2.61 Å to 3.03 Å indicating covalent interactions between Cd and As atoms while the α-phase does not have this distortion. The electron counting can be applied as $(A^{2+})_2(Cd^{2+})(As^{3-})_2$ to understand the charged balanced nature.

Figure 6 shows the structural similarities of both phases. Both have the repeating unit (blue), but an additional $CdAs_4$ tetrahedron is present in the α-phase.

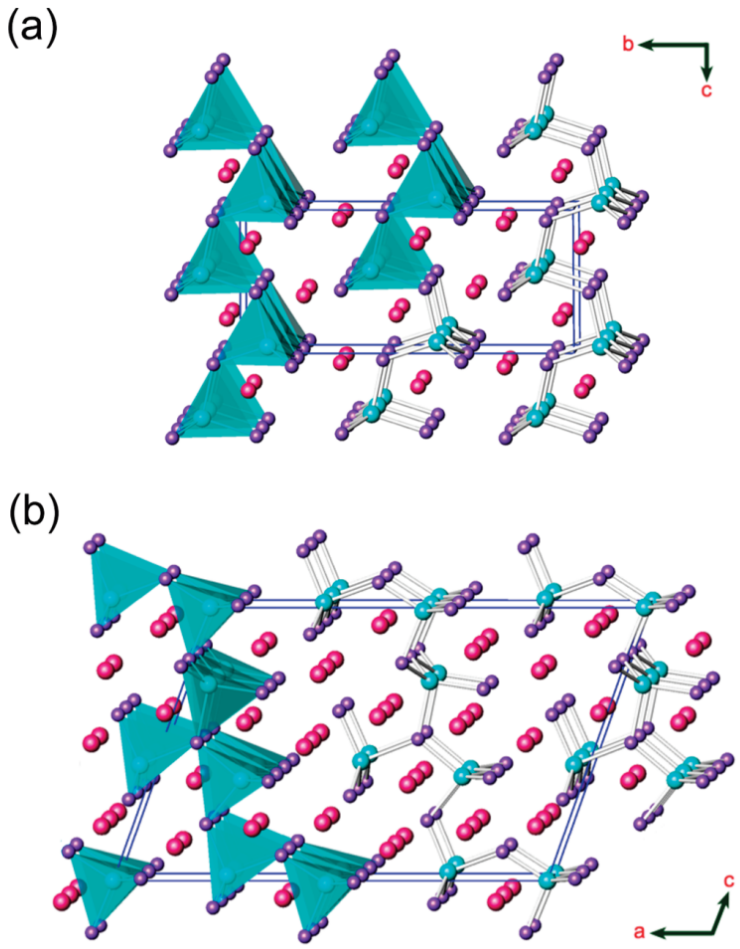

Figure 6. The structure of two polymorphs α-Ca_2CdAs_2 (a) and β-Ca_2CdAs_2 is given. Cd atoms are represented by light blue spheres. They are located at the centers of As_4 tetrahedra (translucent). Purple spheres represent As atoms. Red spheres represent Ca cations. Reprinted from [40] with permission. Copyright 2011 from American Chemical Society.

The differences in structural features have a profound effect on the energy bandgap. Though both compounds show semiconducting behavior with direct bandgap characteristics, the energy difference in bandgap is 0.9 eV in α-Ca_2CdAs_2 and 0.7 eV in β-Ca_2CdAs_2, respectively. This difference could be explained based on the interactions between cations and anions in the structure. There is more distortion in the structure in β-Ca_2CdAs_2 than in α-Ca_2CdAs_2 making the Ca-As bonds slightly less ionic. As a result, the energy gap between the valence and conduction bands is smaller in the β-phase. Other 2-1-2 compositions, Sr_2ZnAs_2 and Ba_2ZnAs_2, are reported to have

ortho-hexagonal structure crystallizing in the $P6_3/mmc$ space group orthorhombic *Ibam* space group respectively.[42]

2.5. $A_2M_2As_3$ (2-2-3)

One more Zintl phase is the composition with the chemical formula $A_2M_2As_3$. Similar to previously discussed compounds, A represents a bivalent cation like Ca, Sr, Ba, Eu, Yb and M represents a transition metal such as Zn or Cd.

$Sr_2Zn_2As_3$ and $Eu_2Zn_2As_3$ crystalize in the monoclinic space group $C2/m$.[43] In this structure shown in Figure 7, chains of corner-sharing MAs_4 tetrahedra form a 1D ribbon. The ribbons are linked through arsenic-arsenic bonds leading to the formation of $[Zn_2As_3]^{4-}$. The ribbons elongate along *b* direction connected by arsenic-arsenic bonds with length 2.49 Å. The cations are present near the arsenic-arsenic bond within the layers. The bonding picture can be rationalized using simple Zintl concept of charged balanced compound as $(A^{2+})_2(Zn^{2+})_2(As^{2-})(As^{3-})_2$. The As1 arsenic atoms share their electrons to form the arsenic-arsenic dimers. They exhibit semiconducting behavior with a narrow band gap of 0.04 eV for $Sr_2Zn_2As_3$ and 0.02 eV for $Eu_2Zn_2As_3$.

One more 2-2-3 composition reported is $Ba_2Cd_2As_3$. The structure is like the $CaAl_2Si_2$ type.[45]

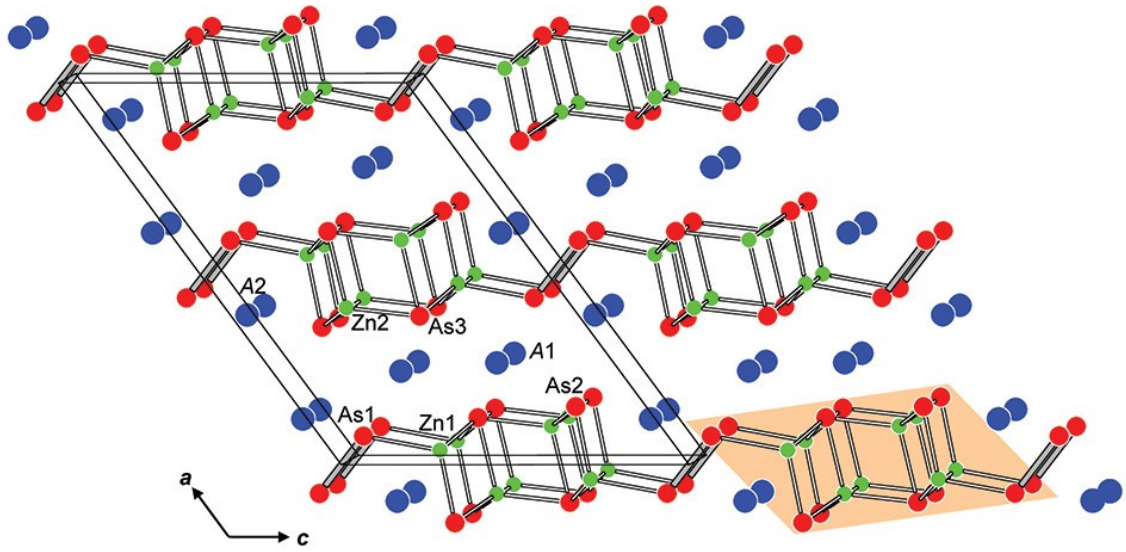

Figure 7. The structure of $A_2M_2As_3$ is presented. Cations (A atoms) are represented by blue circles, M atoms are presented by green circles, and arsenic atoms represented by red circles. Reprinted from [43] with permission. Copyright 2012 from American Chemical Society.

3. Outlook & Conclusion

Arsenic-containing Zintl compounds have the potential as thermoelectric materials with promising efficiencies. The telling structural differences in compositions should be conducive to enabling applications in a wide range of temperatures The intricate relationship among structural, electronic, and phononic properties of these materials paves the way for tuning band gaps, charge carrier concentration, and other properties. Though arsenic-based ternary compounds have been a field of interest for a long time, only a very few Zintl arsenides have been investigated for thermoelectric properties. However, the recent synthesis of new materials could change the trend. One might expect high *zT* based on the structures, similar to the class-leading antimonides.

Thermoelectric materials' efficiency has progressed quickly in the last decade. But the search for the ultimate thermoelectric material with a zT of 3 continues. The advancement in the field depends on discovering new materials and measuring and tuning existing ones. More research on arsenide-based Zintl compounds would help to address the critical issues that hold back practical implementation and mass commercialization of thermoelectric materials.

4. Acknowledgment

The authors acknowledge the contribution of the graduate students, scientists, and the National Science Foundation for continuous support of this research, most recently with grants DMR-2001156 and -2307231.

5. References

[1] S. M. Kauzlarich, S. R. Brown, G. Jeffrey Snyder, *Dalton Transactions* **2007**, 2099–2107.

[2] Q. Yan, M. G. Kanatzidis, *Nat Mater* **2021**, DOI 10.1038/s41563-021-01109-w.

[3] C. J. Perez, G. Cerretti, E. L. K. Wille, K. P. Devlin, N. S. Grewal, A. P. Justl, M. Wood, S. K. Bux, S. M. Kauzlarich, *Chemistry of Materials* **2021**, *33*, 8059–8069.

[4] J. P. A. Makongo, G. M. Darone, S.-Q. Xia, S. Bobev, *J Mater Chem C Mater* **2015**, *3*, 10388–10400.

[5] A. C. Payne, M. M. Olmstead, S. M. Kauzlarich, D. J. Webb, *Chemistry of Materials* **2001**, *13*, 1398–1406.

[6] A. P. Justl, F. Ricci, A. Pike, G. Cerretti, S. K. Bux, G. Hautier, S. M. Kauzlarich, *Sci Adv* **2022**, *8*, eabq3780.

[7] M. Zhong, Q. Xia, L. Pan, Y. Liu, Y. Chen, H.-X. Deng, J. Li, Z. Wei, *Adv Funct Mater* **2018**, *28*, 1802581.

[8] N. C. Norman, *Chemistry of Arsenic, Antimony and Bismuth*, Springer Science & Business Media, **1997**.

[9] M. Zhong, H. Meng, S. Liu, H. Yang, W. Shen, C. Hu, J. Yang, Z. Ren, B. Li, Y. Liu, J. He, Q. Xia, J. Li, Z. Wei, *ACS Nano* **2020**, *15*, 1701–1709.

[10] B. Karki, M. Rajapakse, G. Udaya Sumanasekera, J. B. Jasinski, *ACS Appl Energy Mater* **2020**, *3*, 8543–8551.

[11] Ph. D. James Speight, *Lange's Handbook of Chemistry, Sixteenth Edition*, McGraw-Hill Education, New York, **2005**.

[12] M. Sasaki, S. Horisaka, M. Inoue, *Jpn J Appl Phys* **1987**, *26*, 1704.

[13] S. Singh, P. Dutta, M. Rathi, Y. Yao, Y. Gao, S. Sun, D. Khatiwada, V. Selvamanickam, A. Mavrokefalos, *APL Mater* **2019**, *7*, 031104.

[14] X. Zou, X. Chen, H. Huang, Y. Xu, W. Duan, *Nanoscale* **2015**, *7*, 8776–8781.

[15] N. Soheilnia, H. Xu, H. Zhang, T. M. Tritt, I. Swainson, H. Kleinke, *Chemistry of Materials* **2007**, *19*, 4063–4068.

[16] B. E. Hettick, J. E. Cañas-Carrell, A. D. French, D. M. Klein, *J Agric Food Chem* **2015**, *63*, 7097–7107.

[17] W. G. Zeier, *Curr Opin Green Sustain Chem* **2017**, *4*, 23–28.

[18] H. A. Eivari, Z. Sohbatzadeh, P. Mele, M. H. N. Assadi, *Mater Today Energy* **2021**, *21*, 100744.

[19] S. M. Kauzlarich, A. Zevalkink, E. Toberer, G. J. Snyder, in *Thermoelectric Materials and Devices* (Eds.: I. Nandhakumar, N.M. White, S. Beeby), The Royal Society Of Chemistry, **2016**, p. 0.

[20] H. Schäfer, B. Eisenmann, W. Müller, *Angewandte Chemie International Edition in English* **1973**, *12*, 694–712.

[21] E. Zintl, A. Harder, B. Dauth, *Zeitschrift für Elektrochemie und angewandte physikalische Chemie* **1934**, *40*, 588–593.

[22] G. J. Miller, M. W. Schmidt, F. Wang, T.-S. You, in *Zintl Phases: Principles and Recent Developments* (Ed.: T.F. Fässler), Springer Berlin Heidelberg, Berlin, Heidelberg, **2011**, pp. 1–55.

[23] A. Ovchinnikov, S. Bobev, *J Solid State Chem* **2019**, *270*, 346–359.

[24] G. Cordier, H. Schäfer, *Angewandte Chemie International Edition in English* **1981**, *20*, 466.

[25] A. Bekhti-Siad, K. Bettine, D. P. Rai, Y. Al-Douri, X. Wang, R. Khenata, A. Bouhemadou, C. H. Voon, *Chinese Journal of Physics* **2018**, *56*, 870–879.

[26] S. S. Stoyko, L. H. Voss, H. He, S. Bobev, *Crystals (Basel)* **2015**, *5*, 433–446.

[27] K. Rajput, S. Baranets, S. Bobev, *Chemistry of Materials* **2020**, *32*, 9616–9626.

[28] Z. M. Elqahtani, S. Aman, S. Mehmood, Z. Ali, A. Hussanan, N. Ahmad, S. Alomairy, M. S. Al-Buriahi, Z. A. Alrowaili, H. M. T. Farid, *Journal of Taibah University for Science* **2022**, *16*, 660–669.

[29] M. Radzieowski, F. Stegemann, S. Klenner, Y. Zhang, B. P. T. Fokwa, O. Janka, *Mater Chem Front* **2020**, *4*, 1231–1248.

[30] J. Wang, S.-Q. Xia, X.-T. Tao, *Inorg Chem* **2012**, *51*, 5771–5778.

[31] A. B. Childs, S. Baranets, S. Bobev, *J Solid State Chem* **2019**, *278*, 120889.

[32] D. B. Luo, Y. X. Wang, Y. L. Yan, G. Yang, J. M. Yang, *J Mater Chem A Mater* **2014**, *2*, 15159–15167.

[33] N. Tomitaka, Y. Goto, K. Morino, K. Hoshi, Y. Nakahira, H. Ito, A. Miura, H. Usui, Y. Mizuguchi, *J Mater Chem A Mater* **2021**, *9*, 26362–26370.

[34] P. Verdier, P. L'Haridon, M. Maunaye, Y. Laurent, *Acta Crystallographica Section B* **1976**, *32*, 726–728.

[35] Y. L. Yan, Y. X. Wang, G. B. Zhang, *J Mater Chem* **2012**, *22*, 20284–20290.

[36] A. Rehr, T. Y. Kuromoto, S. M. Kauzlarich, J. Del Castillo, D. J. Webb, *Chemistry of Materials* **2002**, *6*, 93–99.

[37] S. M. Kauzlarich, T. Y. Kuromoto, *Croatica Chemica Acta* **1991**, *64*, 343–352.

[38] S. Baranets, G. M. Darone, S. Bobev, *J Solid State Chem* **2019**, *280*, 120990.

[39] A. V Hoffmann, T. F. Fässler, V. Hlukhyy, *Z Anorg Allg Chem* **2022**, *648*, e202200168.

[40] J. Wang, M. Yang, M.-Y. Pan, S.-Q. Xia, X.-T. Tao, H. He, G. Darone, S. Bobev, *Inorg Chem* **2011**, *50*, 8020–8027.

[41] B. Saparov, S. Bobev, *Inorg Chem* **2010**, *49*, 5173–5179.

[42] D. K. Wilson, B. Saparov, S. Bobev, *Z Anorg Allg Chem* **2011**, *637*, 2018–2025.

[43] S. S. Stoyko, M. Khatun, A. Mar, *Inorg Chem* **2012**, *51*, 2621–2628.

[44] J. Wang, S.-Q. Xia, X.-T. Tao, M. C. Schäfer, S. Bobev, *J Solid State Chem* **2013**, *205*, 116–121.

[45] B. Saparov, H. He, X. Zhang, R. Greene, S. Bobev, *Dalton Transactions* **2010**, *39*, 1063–1070.

[46] G. Cordier, H. Schäfer, M. Steher, *Zeitschrift für Naturforschung B* **1985**, *40*, 1100–1104.

[47] G. Cordier, H. Schäfer, M. Stelter, *Zeitschrift für Naturforschung B* **1987**, *42*, 1268–1272.

[48] B. Eisenmann, H. Jordan, H. Schäfer, *Journal of the Less Common Metals* **1986**, *116*, 251–258.

[49] G. Cordier, H. Schäfer, M. Stelter, *Zeitschrift für Naturforschung B* **1985**, *40*, 5–8.

[50] P. Verdier, P. L'Haridon, M. Maunaye, Y. Laurent, *Acta Crystallographica Section B* **1976**, *32*, 726–728.

[51] J. Hong, O. Delaire, *Materials Today Physics* **2019**, *10*, 100093.

[52] K. P. Devlin, B. Gomez, S. M. Kauzlarich, *Z Anorg Allg Chem* **2022**, *648*, e202100386.

[53] S. M. Kauzlarich, M. M. Thomas, D. A. Odink, M. M. Olmstead, *J Am Chem Soc* **2002**, *113*, 7205–7208.

[54] M. Radzieowski, T. Block, S. Klenner, Y. Zhang, B. P. T. Fokwa, O. Janka, *Inorg Chem Front* **2019**, *6*, 137–147.

[55] T. Vo, P. von Allmen, D. Cheikh, S. Bux, J.-P. Fleurial, *The Journal of Physical Chemistry C* **2022**, *126*, 18490–18504.

[56] J. Wang, M. Yang, M.-Y. Pan, S.-Q. Xia, X.-T. Tao, H. He, G. Darone, S. Bobev, *Inorg Chem* **2011**, *50*, 8020–8027.